Sensors and Actuators B 261 (2018) 279–287

Contents lists available at ScienceDirect

Sensors and Actuators B: Chemical

journal homepage: www.elsevier.com/locate/snb

Two-dimensional molybdenum disulfide (MoS_2) with gold nanoparticles for biosensing of explosives by optical spectroscopy

Jiajia Wu[a], Yanli Lu[a], Zhiqian Wu[b], Shuang Li[a], Qian Zhang[a], Zetao Chen[a], Jing Jiang[c], Shisheng Lin[b], Long Zhu[d], Candong Li[d], Qingjun Liu[a,*]

[a] Biosensor National Special Laboratory, Key Laboratory for Biomedical Engineering of Education Ministry, Department of Biomedical Engineering, Zhejiang University, Hangzhou, 310027, PR China
[b] State Key Laboratory of Modern Optical Instrumentation, Zhejiang University, Hangzhou 310027, PR China
[c] Micro and Nanotechnology Lab, University of Illinois at Urbana-Champaign, IL, 61801 USA
[d] Collaborative Innovation Center of TCM Health Management, Fujian University of Traditional Chinese Medicine, Fuzhou, 350122, PR China

ARTICLE INFO

Article history:
Received 28 September 2017
Received in revised form 6 January 2018
Accepted 21 January 2018

Keywords:
Molybdenum disulfide (MoS_2)
Gold nanoparticle
Biosensor
Peptide
Explosive

ABSTRACT

As one of the most important transition-metal dichalcogenides (TMDs) materials, molybdenum disulfide (MoS_2) has gained extensive attention for its marvelous optoelectronic properties. In this study, nanocomposites of two-dimensional (2D) molybdenum disulfide (MoS_2) with plasmonic noble metal nanoparticles were synthesized by a one-step green process. Under irradiation, 2D MoS_2 in the nanocomposites absorbed photons and generated carriers in a wide spectrum. Then MoS_2 coupled to gold nanoparticles and produced the enhanced electromagnetic field in the nanosturctures, leading to outstanding optical properties. In virtue of bio-compatibilities of the particles, the nanocomposites were chemically modified with specific peptides to construct an optical biosensor for explosive detection. When exposed to 2,4,6-trinitrotoluene (TNT), the biosensor showed significant absorption peak changes in visible spectra with a concentration-dependent behavior. The biosensor could detect TNT at the concentration as low as 2×10^{-7} M. For selectivity, the biosensor could differentiate TNT from other nitroaromatic explosives that have extremely similar structures to TNT, such as 4-nitrotoluene (4-NT) and 2,6-dinitrotoluene (DNT). All the results suggested that the biosensor based on the nanocomposites of 2D MoS_2 coupling to plasmonic nanoparticles exhibited remarkable optical performance, which provided a promising approach to design versatile biosensors to detect biochemical molecules.

1. Introduction

Two-dimensional (2D) materials are an emerging and important class of materials, and have unique physical and chemical properties that drastically differ from their bulk counterparts [1–5]. Many kinds of 2D materials, such as graphene, hexagonal boron nitride, and layered transition metal dichalcogenides (TMDs), have been extensively studied [1,6–9]. In particular, 2D molybdenum disulfide (MoS_2), as one of prototypical layered TMDs, has drew significant attention, due to its extraordinary catalytic, optical, mechanical, and electronic properties [10,11]. The bandgap of MoS_2 ranges from 1.3 to 1.8 eV and exhibits an indirect to direct transition from bulk to monolayer, making them extremely suitable for light absorbents in a wide spectrum [12,13]. However, the light absorption of 2D MoS_2 is considerably weak compared to bulk materials, resulting in limited light-harvest ability [14]. Moreover, without any active group, the pristine 2D MoS_2 sheets are generally difficult to be chemically modified with bio-components to design biosensors [15]. Therefore, efficient utilizations of MoS_2 are still far from the practical optical devices for biosensing. To solve this problem, various strategies have been developed to integrate 2D materials with plasmonic nanomaterials [16–18]. Among those approaches, integration of noble metal nanoparticles with MoS_2 to form hybrid nanostructures of plasmonic metal and 2D MoS_2 has drew extensive attention [19–21].

Owing to unusual chemical and physical properties, especially bio-compatibilities and optical features, noble metal nanoparticles have been widely applied in biosensing systems [22,23]. When combining the nanoparticles with 2D MoS_2 sheets, the plasmonic-electrical effect, including the plasmon-induced "hot electrons", could play a significant role in enhancing optical properties of optic devices [24]. Moreover, the combination of the individual

* Corresponding author.
E-mail address: qjliu@zju.edu.cn (Q. Liu).

https://doi.org/10.1016/j.snb.2018.01.166
0925-4005/

properties, that derived from the noble metal particles and MoS_2 also could provide a multifunctional nanoplatform for various applications [25–27]. Therefore, the nanocomposits of noble metal particles and 2D MoS_2 could take advantages of each nanomaterial to present outstanding optical properties for biosensing.

Several approaches have been proposed to combine MoS_2 with metal nanoparticles. Typically, it was done by either simply mixing the individual constituents, or adding MoS_2 sheets among the metal precursors and reducing agents, to generate nanoparticles on the sheets [28,29]. However, these means often could not achieve chemical bonding or would induce extra reagents in the experiments. Actually, chemically exfoliated MoS_2 sheets have great redox behavior, which could directly reduce metal precursors to allow a very straightforward synthesis of metal-decorated 2D materials sheets, as a green process [30,31].

After integrating MoS_2 with noble metal nanoparticles, the nanocomposites could assemble with a wide variety of biorecognition components, such as nucleic acids, proteins, cells and tissues, through bio-friendly nanoparticles [32–36]. As specific amino acid sequences extracted from proteins, peptides exhibited excellent abilities in biosensing [37,38]. They were easy to be prepared according to standard synthetic protocols. Meanwhile, peptides had great chemical and conformational stability, so they could be preserved for a long time and applied in harsh conditions [39]. In addition, the peptide sequences could be specially designed to bond with different nanomaterials, which made them obtain growing concerns as bio-sensitive elements. For example, explosive-specific peptides have been found and reveal great performance in binding to explosives which are a thorny problem for public security and the environment [40,41]. Meanwhile, explosives are not only an enormous threat for public security, but also major environmental contaminants during the production of shells, bombs and grenades. Obviously, it is of great significance to detect explosives effectively. Therefore, specific peptides can be chosen to assemble with nanocomposites to fabricate biosensors for explosive detection.

In this study, nanocomposites of gold nanoparticles and 2D MoS_2 sheets (AuNPs@MoS_2) were synthesized by a one-step green approach. Theoretical analyses were carried out to confirm the enhanced plasmonic resonance of the nanocomposites. Then the explosive-specific peptides self-assembled on the nanocomposites through Au-S covalent bonds. Thus, a label-free optical biosensor for detection of explosives, such as 2,4,6-trinitrotoluene (TNT), was constructed as a proof-of-concept application. By optical absorption spectra, the biosensor verified the plasmonic resonance of the nanocomposites.

2. Materials and methods

2.1. Synthesis of the AuNPs@MoS_2

To chemically combine MoS_2 and gold nanoparticles, the synthesis was carried out by one-step conjugation in aqueous solvents without any reducing reagent [42]. Then the specific peptides self-assembled on the nanocomposites to form the biosensor for explosive detection. Fig. 1 depicted the overview of the processes to synthesize the nanocomposites and construct the biosensor for TNT detection in this study.

Pristine MoS_2 was composed of covalently bonded S-Mo-S sheets that were bound by weak wan der Waals forces (Fig. 1a). In the synthesis process, 60 mL MoS_2 aqueous dispersion (0.1 mg/mL) from the intercalation-exfoliation was sonicated for 2 h, then was added into a 100 mL Erlenmeyer flask. While the MoS_2 aqueous dispersion under vigorous stirring, Gold (III) tetrachloride trihydrate ($HAuCl_4{\cdot}3H_2O$) was added to it until the concentration of $HAuCl_4$ became 0.01%. After stirring for 10 min under room temperature (~22 °C), the reaction mixture was heated to 60 °C for 5 min. Finally, the nanocomposites of MoS_2 with gold nanoparticles (AuNPs@MoS_2) was purified by centrifugation and stored at 4 °C in an opaque glass container for the sensing studies (Fig. 1b).

For observing the morphology of the nanocomposites, transmission electron microscopy (TEM) images were recorded by JEM-1230 (JEOL, 120 kV). In addition, Raman spectra were performed to further confirm the nanocomposites by Raman spectroscopy (Renishawin ViaReflex) with the excitation wavelength of 532 nm.

At the same time, for comparing the optical performance between AuNPs@MoS_2 and pure gold nanoparticles (AuNPs), AuNPs were prepared based on reduction of $HAuCl_4$ by trisodium citrate ($Na_3C_6H_5O_7$) [43]. Firstly, 10 mL $HAuCl_4$ solution (0.01%) in a 25 mL Erlenmeyer flask was heated to 80 °C, then 185 μL $Na_3C_6H_5O_7$ solution (1%) was added for reduction of the $HAuCl_4$. The heating was kept at 80 °C for 60 min, while the stir was lasted for 75 min. Finally, AuNPs solution was obtained after centrifugation at 3000 r.p.m for 10 min and stored in an opaque glass container at 4 °C for further experiments.

2.2. Theoretical calculations

To clarify the mechanism of interaction between MoS_2 with noble metal nanoparticles, the electric field distribution of the nanocomposites was calculated using the three-dimensional finite-difference time-domain (3D-FDTD) method [44–46].

In this calculation model, two AuNPs with a gap of 2 nm on a MoS_2 sheet in aqueous solution illuminated by a linearly polarized plane wave with an electric field amplitude of 1 V/m. The diameter of the AuNPs, thicknesses of the MoS_2 sheet, and the Yee cell size were 30, 2.5, and $1 \times 1 \times 1$ nm, respectively. Moreover, the refractive indexes of solution and MoS_2 used here were 1.3 and $5.2 + 1.2i$ [47,48]. For comparison, the electric field distribution of pure AuNPs with same parameters was simulated. All the calculations were performed using commercially available Lumerical FDTD Solutions software (Lumerical Solutions, Inc. Vancouver, Canada). The theoretical calculations of the nanocomposites' optical performance were then analyzed with the spectra to guide the design of the biosensor.

2.3. Optical measurements

Visible absorption spectra were performed to characterize the nanocomposites and detected explosives by a spectrophotometer (USB2000+, Ocean Optics Inc, Dunedin, USA) with 0.38 nm optical path.

The spectrophotometer was calibrated with light intensity and other parameters to prevent light saturation, and the reference spectra were recorded before every trial. Then the absorption spectra from 400 nm to 700 nm of those solutions in cuvettes were measured. Finally, the plasmonic peaks of samples were read in the spectra as the statistical data to analyze the results.

2.4. Bio-functionalization of the nanocomposites

To equip the nanocomposites with the ability to detect explosives, peptides were chosen as the bio-recognition components to modify AuNPs@MoS_2. As a typical explosive, TNT was chosen as the targets for explosive detection in this system.

The TNT-specific peptide chain (WHWQRPLMPVSIC) was designed based on reports about TNT-specific amino acids [40,49]. Peptides were synthesized with solid phase peptide synthesis (SPSS) by stepwise addition of protected amino acids to growing peptide chains. The quality of the synthesized peptides was tested by high-performance liquid chromatography (HPLC) and

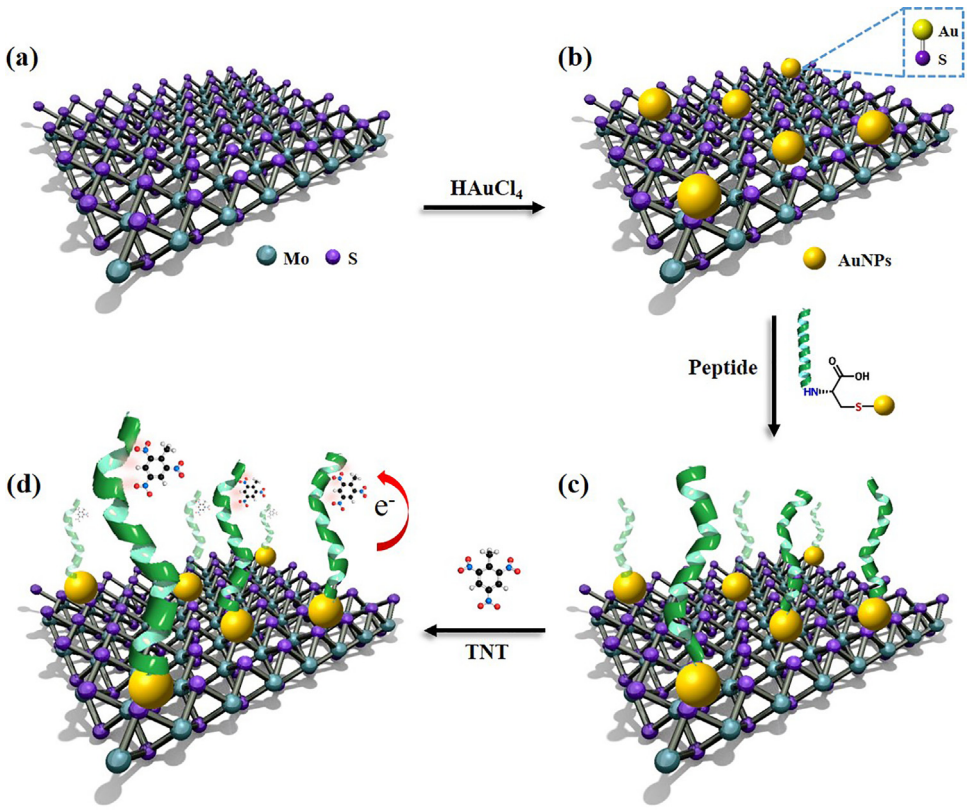

Fig. 1. The construction process of the biosensor based on the nanocomposites for explosive detection. (a) The pristine MoS_2 sheets. (b) Hybrid nanostructures of AuNPs@MoS_2 were synthesized by one-step conjugation. (c) The TNT-specific peptides which designed with sulfydryl groups were immobilized on AuNPs@MoS_2 through Au-S covalent bonds. (d) The biosensor could capture TNT molecules and induce absorption peak changes.

mass spectrum (MS). Then the peptides were dissolved in phosphate buffer solution (PBS, 0.1 M, pH 7.2) at 1 mg/mL for composites bio-functionalization.

For assembling the nanocomposites with peptides, 10 mL freshly prepared AuNPs@MoS_2 solution was adjusted to pH 8.0 with sodium hydroxide (NaOH), then 100 μL TNT-specific peptides (1 mg/mL) was added. The mixture preserved at 4 °C in the dark for 12 h for assembling the peptides with gold particles through Au-S covalent bonds. Then the mixture was centrifuged at 6400 r.p.m for 30 min at 4 °C to remove unbound peptides. The sediment was then redispersed in deionized water and the centrifugation process repeated several times to guarantee a relatively pure aqueous solution of peptide-functionalized AuNPs@MoS_2 (Fig. 1c).Then same steps were performed on pure AuNPs and pristine MoS_2 (0.1 mg/mL) as well.

2.5. Explosive detections

The charge-transfer interactions happened between the peptides and explosive molecules, which could invoke optical absorption changes (Fig. 1d). So optical spectra could record the absorption peaks of the biosensor toward different concentrations of explosives for detection.

Firstly, TNT was diluted into nine different concentrations (2×10^{-7}, 4×10^{-7}, 1×10^{-6}, 2×10^{-6}, 4×10^{-6}, 1×10^{-5}, 2×10^{-5}, 4×10^{-5}, 1×10^{-4} M) with anhydrous methanol. Then 20 μL different concentrations of TNT were added to the peptide-functionalized AuNPs@MoS_2 (200 μL) respectively. Anhydrous methanol (20 μL) was also added to the peptide-functionalized AuNPs@MoS_2 as the control trial. To confirm the function of TNT-specific peptides, AuNPs@MoS_2 without being functionalized were used to detect TNT solutions (4×10^{-7}, 2×10^{-6}, 4×10^{-6}, 2×10^{-5}, 4×10^{-5} M) by repeating the same procedures. In addition, to compare the performance of AuNPs@MoS_2, pure AuNPs, and pristine MoS_2 for TNT detection, same steps were performed to detect TNT using functionalized AuNPs and MoS_2.

To evaluate the specificity of the biosensor, 4-NT and DNT were chosen to be detected with the biosensor, because they were also nitroaromatic explosives which were the analogues of TNT. 4-NT and DNT were dissolved in anhydrous methanol at five concentrations (4×10^{-7}, 2×10^{-6}, 4×10^{-6}, 2×10^{-5}, 4×10^{-5} M). Same operation steps were repeated for detection of 4-NT and DNT. In addition, the stability of the biosensor was also tested with the same procedures. 48 mL AuNPs@MoS_2 was functionalized with peptides on the first day, then in the following days, 3 mL AuNPs@MoS_2 solution was daily removed and centrifuged at 6400 r.p.m for 30 min at 4 °C to remove unbound peptides. The sediment was then redispersed in deionized water and the centrifugation process repeated several times to guarantee a relatively pure aqueous solution of peptide-functionalized AuNPs@MoS_2. These functionalized nanocomposites then were used to detect 4×10^{-6} M TNT, which lasted for 16 days so as to test the stability of the biosensor.

Except that few-layer MoS_2 purchased from XFNANO Materials Tech Co., Ltd. (Nanjing, China), all the other reagents were obtained from Sigma-Aldrich Co., LLC. Besides, all the experiments were performed at the room temperature (~22 °C) unless otherwise noted.

3. Results

3.1. MoS_2 coupling to plasmonic nanoparticles

To identify the reaction products, optical spectra of the $HAuCl_4$, pristine MoS_2, and the reaction products were recorded. Absorption spectra of $HAuCl_4$ and MoS_2 showed that the MoS_2 dispersion

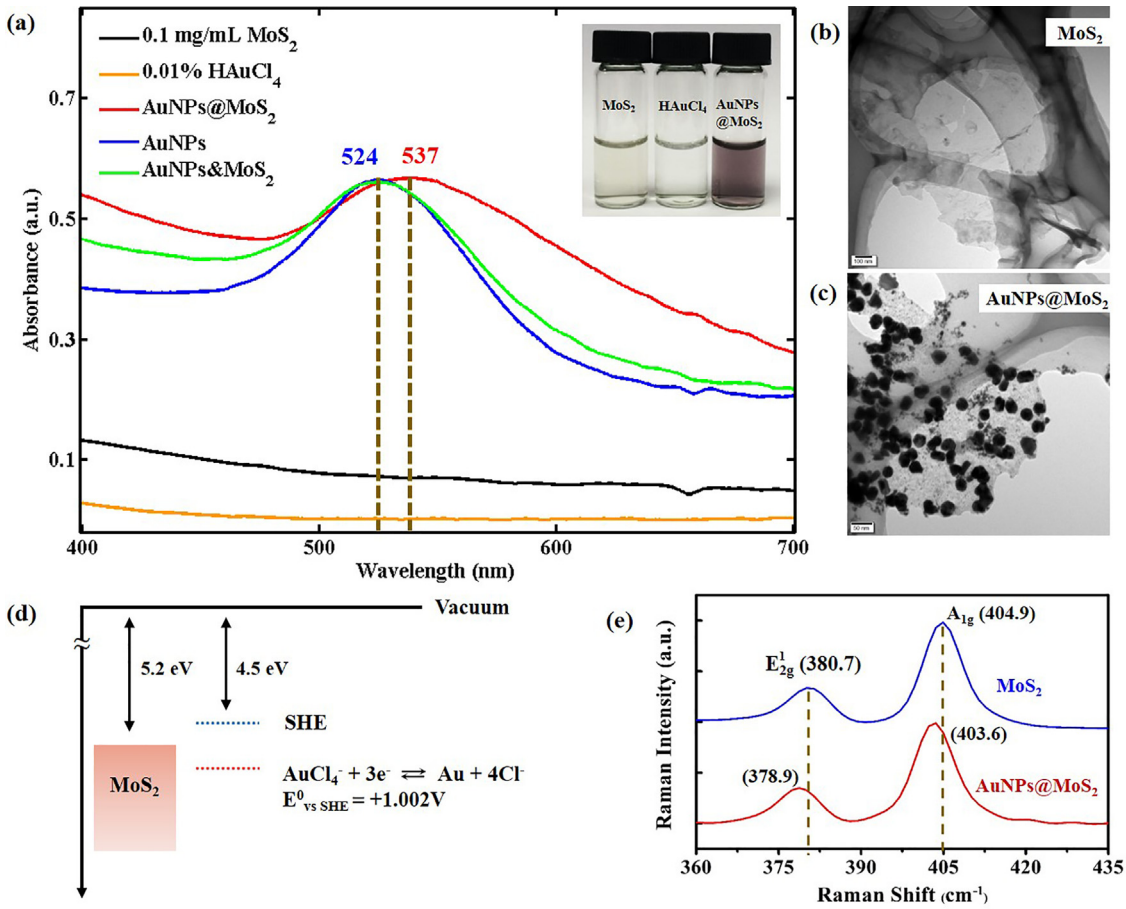

Fig. 2. Characterization of the nanocomposites. (a) Absorption spectra of pristine MoS_2 (0.1 mg/mL), $HAuCl_4$ (0.01%), synthesized AuNPs@MoS_2, AuNPs, physical-blended AuNPs and MoS_2 (AuNPs&MoS_2). Inset: pictures of the MoS_2 sheets, $HAuCl_4$ and AuNPs@MoS_2. (b), (c) TEM images of pristine MoS_2 sheets and synthesized AuNPs@MoS_2, showed a MoS_2 sheet uniformly decorated by AuNPs. (d) An energy diagram showed that the Fermi level of MoS_2 lay above the reduction potential of $AuCl_4^-$, which suggested that a spontaneous redox reaction can occur between MoS_2 and $HAuCl_4$. (e) Raman spectra of pristine MoS_2 and AuNPs@MoS_2.

and gold precursor had no obvious absorption peak in the visible region. After $HAuCl_4$ was added to MoS_2 aqueous dispersion, an evident color change was observed as the dispersion changed from pale yellow to purple (Fig. 2a, inset). Meanwhile, a new distinctive absorption peak corresponding to the Au plasmonic resonant peak in the spectrum at around 536 nm emerged, suggesting the formation of gold nanoparticles (Fig. 2a). Therefore, absorption spectra showed the plasmonic resonance peaks of the nanocomposites of MoS_2 and gold nanoparticles.

At the same time, TEM results of pristine MoS_2 sheets and the nanocomposites showed that gold nanoparticles uniformly decorated both the edges and basal planes of the MoS_2 layers, which indicated that $HAuCl_4$ could spontaneously react with MoS_2 and be reduced to gold nanoparticles (Fig. 2b, c). The mechanism was likely due to the redox reactions between MoS_2 and $AuCl_4^-$ [30,50]. The work function of MoS_2 was 5.2 eV, situating the Fermi level of MoS_2 well above the reduction potential of $AuCl_4^-$ (+1.002 V versus the standard hydrogen electrode (SHE), Fig. 2d). Therefore, MoS_2 and $AuCl_4^-$ would form a redox pair, allowing spontaneous electron transfer from MoS_2 to $AuCl_4^-$ and leading to the formation of gold nanoparticles. In addition, from TEM images and the size distribution of AuNPs, the average diameter of AuNPs in the nanocomposites was about 30 nm. However, pure gold nanoparticles of 30 nm and AuNPs&MoS_2 mixture both exhibited a peak at wavelength of ~524 nm in the spectra (Fig. 2a). Thus, owing to the chemical hybrid nanostructure of MoS_2 and gold nanoparticles, the nanocomposites showed unique optic properties that differed from pure AuNPs and physical blend of two substances.

To further reveal the molecular structure of the nanocomposites, Raman spectra were also performed. As shown in Fig. 2e, the pristine MoS_2 produced two representative vibration peaks, $E_{2g}{}^1$ and A_{1g}. The $E_{2g}{}^1$ phonon mode (~380 cm^{-1}) represented in-plane vibrations of Mo and S atoms, whereas the A_{1g} phonon mode (~404 cm^{-1}) represented the out-of-plane vibration of S atoms. The frequency difference of the $E_{2g}{}^1$ and A_{1g} peaks was about 24 cm^{-1}, which rendered that the MoS_2 sheets were few-layer [51,52]. Upon decoration of pristine MoS_2 with Au nanoparticles, the $E_{2g}{}^1$ and A_{1g} modes red shifted by ~1.5 cm^{-1}, suggesting MoS_2 were n-type doped by AuNPs [53]. What all the above indicated was that the gold nanoparticles were successfully decorated on the surface of MoS_2 nanosheets and became composites of AuNPs@MoS_2.

3.2. Optical properties of the nanocomposites

To investigate the optical properties of the nanocomposites under irradiation at ambient conditions, 3D-FDTD method was used to calculate the electric field distribution according to its physical nanostructure.

As shown in Fig. 3a, when the light irradiated on the surface of pure AuNPs, the free electrons underwent oscillation along the axis of two nanoparticles paralleled to the surface. A large amount of free electrons were involved in the oscillation in this dipole direction, then a strong electric field emerged in the gap of the two nanoparticles (Fig. 3b).

Furthermore, as Fig. 3c showed, when the MoS_2 sheet contacted with AuNPs, the dipole interactions led to a partial positive field at

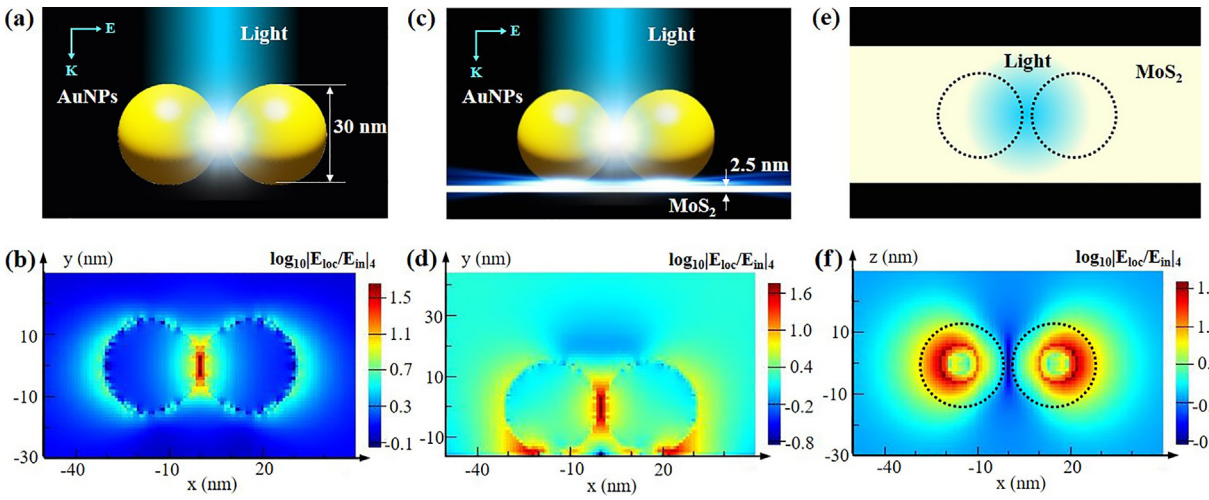

Fig. 3. Electric field distribution of pure AuNPs and AuNPs@MoS_2 at the same condition. (a) Scheme of the pure AuNPs calculation model with two AuNPs with a gap of 2 nm. (b) Electric field distribution of the pure AuNPs model. (c) Scheme of the AuNPs@MoS_2 calculation model that a MoS_2 sheet of 2.5 nm was added under two AuNPs. (d) Electric field distribution in accordance with the AuNPs@MoS_2 model. (e) Top view of the MoS_2 sheet in the AuNPs@MoS_2 model. (f) Electric field distribution on the MoS_2 sheet.

the bottom of the particles, and a few free electrons in the MoS_2 sheet reservoir were induced to gather under the nanoparticles as a result of the electrostatic effect. Then, the redistribution of electrons/dipoles would occur. Fig. 3d showed such a redistribution due to the competition between the coupling of nanoparticles and the coupling of the MoS_2 sheet with nanoparticles. In this case, the electrons were confined at two positions, with similar surface charge density. Then the distribution of electrons/dipoles in a specific metal structure finally reached a state in phase with the wavelength of excitation light. The free electrons gathered at the bottom of nanoparticles to form a relatively stronger nearfield coupling to the MoS_2 sheet. The top-down view showed the distribution on MoS_2 sheet in the steady state of the gold dimer-film system excited at 537 nm (Fig. 3e, f).

By comparing Fig. 3b and d, it could be found that there were more strongly enhanced positions (so-called hot spots) locating in the structure of the composites. More hot spots meant the plasmonic resonance of the nanocomposites was more violent. Therefore, AuNPs@MoS_2 exhibited excellent optical properties, which could be used to fabricate useful optical biosensors.

3.3. The nanocomposites functionalized with peptides

As a bio-recognition component, the TNT-specific peptides used here were especially designed with a cysteine at the carboxy terminus, while the cysteine had a sulfydryl group. The HPLC and MS results indicated the successful synthesis of the TNT-specific peptides (Fig. S1).

Through the covalent bonds of gold nanoparticles with the sulfydryl groups, the peptides self-assembled on the nanoposites easily, to achieve the peptides self-assembled biosensor without additional linkage. In addition, the absorption peak of the nanocomposites red-shifted ~4 nm after binding with the TNT-specific peptides (Fig. 4). Several studies suggested that the shift in absorbance peak was usually caused by the changes in molecular structure of the substances, which altered its refractive index [54–56]. So it's speculated that peptides could lead the refractive index of the AuNPs on nanocomposites to change. The shift also indicated that TNT-specific peptides had been crosslinked to AuNPs@MoS_2, which made the functionalized AuNPs@MoS_2 show structural differences from the bare nanocomposites.

As a result, the peptides self-assembled biosensor for TNT detection was constructed. To verify the experimental principles,

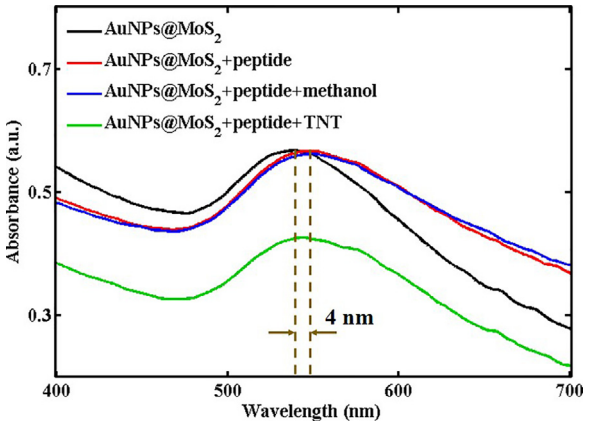

Fig. 4. Absorption spectra showed that the absorption peak of peptides-functionalized AuNPs@MoS_2 had a red shift in the wavelength. However, methanol could not change the absorption peak which decreased after peptides-functionalized nanocomposites toward TNT (4×10^{-6} M). (For interpretation of the references to colour in this figure legend, the reader is referred to the web version of this article.)

20 μL 4×10^{-6} M TNT solution was added to 200 μL functionalized nanocomposites. The absorption peak of the biosensor toward methanol did not change but did decrease with the TNT solution, which confirmed the feasibility of the biosensor (Fig. 4). Therefore, we chose changes of the spectrum peaks, the difference between the control group and the test group, as signals for explosive detection.

3.4. Explosive detection by the biosensor

TNT-specific peptides had the ability to recognize trace amounts of TNT through multivalent binding. So the biosensor could capture TNT molecules in the aqueous environment.

When different concentrations of TNT were added to react with the biosensor respectively, the absorption peak value at the wavelength of 541 nm changed significantly compared to the control trial of methanol, implying that interactions occurred between TNT molecules and the peptides on the nanocomposites. As a result, those absorbance peak changes could be employed for quantitative analysis. The absorption peak value decreased linearly when the concentrations of TNT ranged from 2×10^{-7} M to 1×10^{-4} M

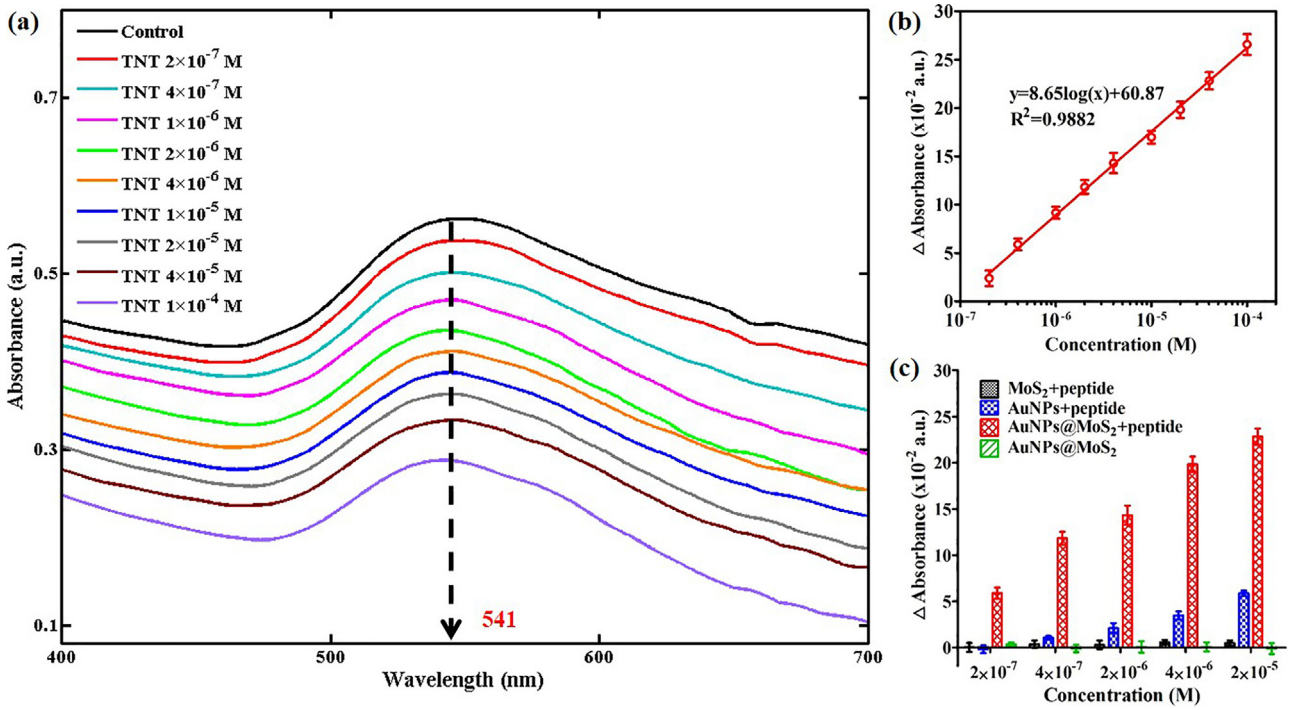

Fig. 5. Measurement of TNT using the optical biosensor. (a) The absorption spectra of the biosensor with TNT at different concentrations. (b) Concentration-dependent curves of peak-value changes read from absorption spectra. (c) Statistics of the performance of functionalized AuNPs@MoS_2, MoS_2, AuNPs and bare AuNPs@MoS_2 in TNT detection (mean ± SD, n = 5).

(Fig. 5a). Moreover, the concentration-dependent curve for TNT could be fitted into linear relationship of y = 8.65log(x) + 60.87, where x and y represented the concentrations of TNT and their peak-value changes, respectively. Besides, small standard deviations (SDs) could be seen in the statistical results, suggesting the reproducibility for TNT detection (R^2 = 0.9882) (Fig. 5b). Thus, the biosensor exhibited an outstanding ability in TNT detection, which indicated a promising approach for rapid and quantitative tests of explosives.

To further confirm the preeminent performance of the biosensor, peptides-functionalized gold nanoparticles and MoS_2 respectively were used to detect TNT molecules as well. MoS_2 with peptides showed no obvious responses to any concentrations of TNT, because MoS_2 nanosheets lacked plasmonic peaks that could be influenced by TNT (Fig. 5c). As Fig. S2 shown, gold nanoparticles have an absorption peak at ~524 nm in the spectrum and red-shift to ~527 nm with TNT-specific peptides, due to the refractive index changes caused by the peptides. The absorption peak value also changed after addition of TNT solutions to peptides-functionalized gold nanoparticles and showed a linear relationship. However, from the absorption spectra comparison and statistical responses of the peak-value changes, the valid signals of the biosensor based on AuNPs were only in a smaller magnitude than those from AuNPs@MoS_2 (Fig. 5c). The biosensor based on AuNPs@MoS_2 exhibited higher sensitivity to TNT. It revealed that AuNPs@MoS_2 showed preferable optical properties than gold nanoparticles and naturally magnify the responses to TNT, corresponding to the 3D-FDTD calculations above.

For certifying the function of TNT-specific peptides, AuNPs@MoS_2 without the peptides were applied in TNT detection for comparison with the same procedure. As Fig. 5c showed, without peptides, the peak value didn't change according to the variation of TNT concentrations, while functionalized AuNPs@MoS_2 exhibited an excellent linear relationship with the logarithm of TNT concentrations. Hence, it indicated that the sensitivity of the biosensor was really from the specific conjunction between peptides and TNT molecules.

Besides TNT, the other two nitroaromatic compounds, 4-NT and DNT, which are often found in explosives, were chosen for the specificity experiments. Fig. 6a showed statistics results for the absorption peak-value changes of TNT, DNT, and 4-NT groups in the spectra. For three explosive targets at increasing concentrations, the biosensor had a significant concentration-dependent behavior to TNT. However, the biosensor only showed slight responses to DNT, while 4-NT almost elicited no response. Therefore, the biosensor displayed high selectivity to TNT and could not be interfered by other compounds such as DNT and 4-NT. Moreover, as Fig. 6b showed, the changes of absorption spectra of the biosensor began to decrease on the eleventh day, which meat the biosensor's responses to TNT molecules began to decline.

4. Discussion

4.1. The green synthesis of the nanocomposites

The combination of noble metal nanomaterials and MoS_2 has been a research upsurge in many fields owing to its excellent properties [20,57,58]. However, physical blend of these two class materials could cause the instability of the detection, while chemical reaction often induced impurity. In this study, the synthesis made full use of the reducibility of chemically exfoliated MoS_2 sheets without any other reagent. The characterization results of visible spectra, TEM images, and Raman spectra showed AuNPs@MoS_2 were chemically synthesized (Fig. 2). It indicated that chemically exfoliated MoS_2 sheets did have the reducing properties that differed from unabridged MoS_2 sheets. Therefore, this synthesis process was green and easy to manipulate.

At the same time, some studies have reported that MoS_2 sheets made from the intercalation-exfoliation method had abundant defects, which can lead to ligand conjugation of MoS_2 [59,60]. In

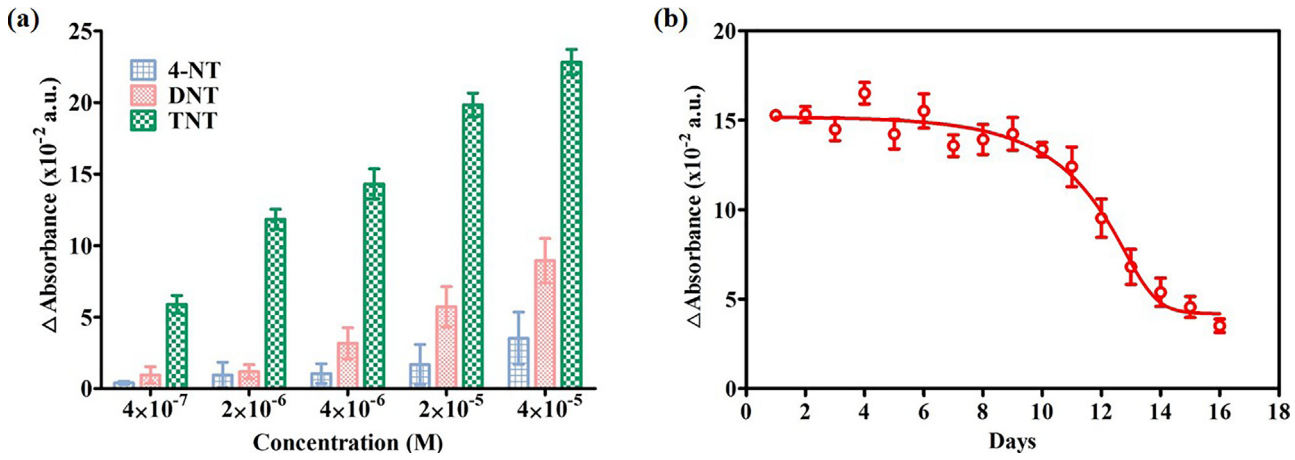

Fig. 6. The selectivity and stability of the biosensor. (a) Selectivity analysis of the biosensor responses to 4-NT, DNT, and TNT (mean ± SD, n = 5). (b) The biosensor based on AuNPs@MoS_2 detected 4×10^{-6} M TNT for 16 days to test the stability of the sensor (mean ± SD, n = 3).

this work, AuNPs bound with naked S atoms through Au-S covalent bonds in AuNPs@MoS_2, which was confirmed by Raman spectrum (Fig. S3). There was a peak at 278 cm^{-1} at the Raman spectrum, which was consistent with the Au-S bond typical peak of Raman spectra [61].The stable covalent bonds prevented the inconsistency of the nanocomposites and improved the stability of the system. A great deal of TMDs similar to MoS_2 are gaining increasing attention for their unique performance, so this green and one-step combination can also be referenced to produce novel nanohybrids for various applications.

4.2. Optical properties of the nanocomposites enhanced by coupling electromagnetic field

As reported in many studies, nanocomposites often exhibited improved optical properties [62,63]. The synthesized AuNPs@MoS_2 nanocomposites also showed outstanding optical properties, which was confirmed by both 3D-FDTD calculations and biosensing results (Figs. 3 and 6). That was because few-layer MoS_2 could absorb photons in a wide spectrum and produce carriers. Then the local dielectric constant was altered due to the interactions of the electromagnetic field around gold nanoparticles with the continuum of delocalized propagation surface plasmon at the underlying MoS_2 surface, thus leading to a high localization of the electric field in the gap between the particles and the MoS_2 surface. In addition, TMDs materials could dephase the oscillation frequency of the free electrons of gold nanoparticles [64]. So the nanocomposites presented a plasmonic peak at the wavelength of 537 nm other than 524 nm of pure gold nanoparticles. Furthermore, compared with that based on gold nanoparticles, the biosensor based on AuNPs@MoS_2 exhibited higher sensitivity, due to the improved optical performance. With the violent electromagnetic coupling phenomenon in the nanostructure, the biosensor's responses to the same excitation would be more obvious, which can be applied as novel substrates in a wide variety of optical sensors.

4.3. The bio-functionalization and detection performance of the biosensor

The plasmonic biosensor based on AuNPs@MoS_2 for TNT detection was proposed in this study where AuNPs@MoS_2 were used as sensor substrate and TNT-specific peptides were employed as biosensitive components. TNT-specific peptides (WHWQRPLMPVSIC) used here were specially designed for this biosensor [40,49]. While WHWQRPLMPVSI was the valid peptide chain sensitive to TNT molecules, a cysteine acid was added at the carboxy terminus of the peptide chain as 'linking residue' tail. Since cysteine had a sulfydryl group, the peptide chain could generate a covalent bond of Au-S on the surface of AuNPs@MoS_2. Therefore, peptides self-assembled on AuNPs@MoS_2 through Au-S covalent bonds, and the red-shift of the absorption peaks in visible spectra proved the successful functionalization (Fig. 4). In addition, the peptides used here could be designed by synthetic chemistry to have various artificial selectivity and be used for different bio-detections [38,65].

It was reported that the specific binding of peptides with TNT molecules might be evoked by the donor-acceptor interactions between tryptophan and TNT, π-π interactions between histidine and TNT, and partial charge-charge interactions or hydrogen bonds between imidazole side chains in peptides and nitro groups in TNT molecules [40,66,67]. Especially, reports confirmed that 2,4,6-Trinitrophenol (TNP), a chemical extremely similar to TNT, could be connected with imidazolylmethylpyrene via several C—H—π, π—π stacking interactions [68]. Therefore, the charge exchange between TNT molecules and peptide chains on AuNPs@MoS_2 affected the local electronic distribution and nearfield coupling between AuNPs and MoS_2 of the nanocomposites, which induced the absorption-peak changes of the biosensor. Those changes depended on the strength of charge-transfer interactions. So the optical biosensor based on AuNPs@MoS_2 demonstrated outstanding performance in quantifying interactions between TNT and peptides with high sensitivity, real-time response, and label-free detection.

Furthermore, the selectivity analysis showed that the biosensor had low responses to DNT, and no response to 4-NT. It might be due to the adjacent methyl and nitro groups of molecular structure of DNT, which had electron interactions with tryptophan and histidine on peptides and generated absorption peak-value changes. However, 4-NT had no conjunction with the peptides and was unable to elicit resonance changes. Those results were in accordance with previous studies that these TNT-specific peptides could also respond to DNT because of the similar structure of DNT to TNT, but responses were much less evident compared with TNT [40,69]. Thus, this biosensor could distinguish TNT molecules among other substances, such as 4-NT and DNT. Additionally, the Au-S covalent bonds were very stable, so the biosensor could maintain the sensitivity to TNT molecules more than ten days (Fig. 6b). After the eleventh day, peptides might begin to hydrolyze and be oxidized, which could lead to the inactivation of the biosensor. Overall, the biosensor showed eminent robustness and stability in TNT discrimination and could satisfy the requirement of practical applications.

The novel nanocomposites AuNPs@MoS_2 played a vital role in the biosensor for detecting TNT. 2D MoS_2 have extraordinary properties to absorb light in a wide spectrum. Meanwhile, AuNPs show

outstanding performance in bio-compatibilities. The nanocomposites took advantages of both materials, then the coupling effect resulted in the enhanced electromagnetic field and magnified the biosensor's responses to the explosives. Therefore, compared with AuNPs (Figs. 3, 5c, S2), AuNPs@MoS_2 significantly improved the sensitivity of the biosensor for explosive detection.

As a result, our study provides a promising approach to detect explosives by combining nanocomposites of MoS_2 and nanoparticles with specific peptides. Actually, similar to the peptides, there are a variety of bio-components and receptors for sensitively capturing targets, such as DNA strands, antibodies, cells and tissues, and they all can be functionalized to nanocomposites for biosensing. Moreover, it has been reported that MoS_2 shows excellent fluorescence quenching capabilities, which makes it possible for fluorescence measurements to be applied for various purposes with the MoS_2 nanocomposites [70]. It's also promising to synthesize MoS_2-derived chemicals that not only could provide fluorescent signals, but also could specifically detect targets [68]. In addition, peptides are able to respond to gas-phase molecules [40], which means it is possible to specifically detect molecules in the air with improved detection systems. Hence, with further development of materials and bio-technology, this kind of biosensing systems based on MoS_2 can be extensively used for pathogen detection, pollutants monitoring, and disease diagnosis.

5. Conclusion

In summary, the hybrid nanostructures of few-layer MoS_2 with plasmonic gold nanoparticles were successfully synthesized by a green and one-step process. The nanocomposites exhibited extraordinary optical properties due to the photon-absorption of MoS_2 and the electromagnetic field coupling between MoS_2 and gold nanoparticles. Based on that, we constructed an optical biosensor with the nanocomposites and specific peptides for detecting explosives. Through spectroscopic observation, the biosensor showed high sensitivity, specificity, and stability in TNT detection. Thus, by combining with various bio-components, nanocomposites of MoS_2 with different nanoparticles could provide a promising approach to develop versatile biosensors.

Acknowledgments

This work was supported by the National Natural Science Foundation of China (Grant No. 31671007), the Zhejiang Provincial Natural Science Foundation of China (Grant No. LZ18C100001) and the Collaborative Innovation Center of Traditional Chinese Medicine Health Management of Fujian province of China.

Appendix A. Supplementary data

Supplementary data associated with this article can be found, in the online version, at https://doi.org/10.1016/j.snb.2018.01.166.

References

[1] K.F. Mak, J. Shan, Photonics and optoelectronics of 2D semiconductor transition metal dichalcogenides, Nat. Photonics 10 (2016) 216–226.
[2] M. Chhowalla, H.S. Shin, G. Eda, L.-J. Li, K.P. Loh, H. Zhang, The chemistry of two-dimensional layered transition metal dichalcogenide nanosheets, Nat. Chem. 5 (2013) 263–275.
[3] X. Xu, W. Yao, D. Xiao, T.F. Heinz, Spin and pseudospins in layered transition metal dichalcogenides, Nat. Phys. 10 (2014) 343–350.
[4] A.K. Geim, K.S. Novoselov, The rise of graphene, Nat. Mater. 6 (2007) 183–191.
[5] Y. Zhang, Y.-W. Tan, H.L. Stormer, P. Kim, Experimental Observation of Quantum Hall Effect and Berry's Phase in Graphene, arXiv preprint cond-mat/0509355, 2005.
[6] C. Tan, X. Cao, X.-J. Wu, Q. He, J. Yang, X. Zhang, J. Chen, W. Zhao, S. Han, G.-H. Nam, Recent advances in ultrathin two-dimensional nanomaterials, Chem. Rev. 117 (2017) 6225–6331.
[7] R. Raccichini, A. Varzi, S. Passerini, B. Scrosati, The role of graphene for electrochemical energy storage, Nat. Mater. 14 (2015) 271.
[8] F. Bonaccorso, L. Colombo, G. Yu, M. Stoller, V. Tozzini, A.C. Ferrari, R.S. Ruoff, V. Pellegrini, Graphene, related two-dimensional crystals, and hybrid systems for energy conversion and storage, Science 347 (2015) 1246501.
[9] S. Berweger, S. Zhiwen, H.A. Bechtel, S. Yinghui, Z. Bo, J. Chenhao, C. Henry, M.C. Martin, M.B. Raschke, F. Wang, Amplitude and phase-resolved nano-spectral imaging of surface phonon polaritons in hexagonal boron nitride, Nano Lett. 2 (2015).
[10] R. Ganatra, Q. Zhang, Few-layer MoS2: a promising layered semiconductor, ACS Nano 8 (2014) 4074–4099.
[11] H. Zeng, J. Dai, W. Yao, D. Xiao, X. Cui, Valley polarization in MoS2 monolayers by optical pumping, Nat. Nanotechnol. 7 (2012) 490–493.
[12] K. He, C. Poole, K.F. Mak, J. Shan, Experimental demonstration of continuous electronic structure tuning via strain in atomically thin MoS2, Nano Lett. 13 (2013) 2931–2936.
[13] A. Splendiani, L. Sun, Y. Zhang, T. Li, J. Kim, C.-Y. Chim, G. Galli, F. Wang, Emerging photoluminescence in monolayer MoS2, Nano Lett. 10 (2010) 1271–1275.
[14] M.-L. Tsai, S.-H. Su, J.-K. Chang, D.-S. Tsai, C.-H. Chen, C.-I. Wu, L.-J. Li, L.-J. Chen, J.-H. He, Monolayer MoS2 heterojunction solar cells, ACS Nano 8 (2014) 8317–8322.
[15] Q. Ding, K.J. Czech, Y. Zhao, J. Zhai, R.J. Hamers, J.C. Wright, S. Jin, Basal-plane ligand functionalization on semiconducting 2H-MoS2 monolayers, ACS Appl. Mater. Interfaces 9 (2017) 12734–12742.
[16] B. Mukherjee, N. Kaushik, R.P. Tripathi, A. Joseph, P. Mohapatra, S. Dhar, B. Singh, G.P. Kumar, E. Simsek, S. Lodha, Exciton emission intensity modulation of monolayer MoS2 via Au plasmon coupling, Sci. Rep. 7 (2017) 41175.
[17] S. Butun, S. Tongay, K. Aydin, Enhanced light emission from large-area monolayer MoS2 using plasmonic nanodisc arrays, Nano Lett. 15 (2015) 2700–2704.
[18] Y. Li, Z. Li, C. Chi, H. Shan, L. Zheng, Z. Fang, Plasmonics of 2D nanomaterials: properties and applications, Adv. Sci. 4 (2017) 1600430.
[19] L. Jin, Z. Meng, Y. Zhang, S. Cai, Z. Zhang, C. Li, L. Shang, Y. Shen, Ultrasmall Pt nanoclusters as robust peroxidase mimics for colorimetric detection of glucose in human serum, ACS Appl. Mater. Interfaces 9 (2017) 10027–10033.
[20] S. Su, M. Zou, H. Zhao, C. Yuan, Y. Xu, C. Zhang, L. Wang, C. Fan, L. Wang, Shape-controlled gold nanoparticles supported on MoS 2 nanosheets: synergistic effect of thionine and MoS 2 and their application for electrochemical label-free immunosensing, Nanoscale 7 (2015) 19129–19135.
[21] P. Zuo, L. Jiang, X. Li, B. Li, Y. Xu, X. Shi, P. Ran, T. Ma, D. Li, L. Qu, Shape-Controllable gold Nanoparticle–MoS2 hybrids prepared by tuning edge-active sites and surface structures of MoS2 via temporally shaped femtosecond pulses, ACS Appl. Mater. Interfaces 9 (2017) 7447–7455.
[22] S. Zeng, K.-T. Yong, I. Roy, X.-Q. Dinh, X. Yu, F. Luan, A review on functionalized gold nanoparticles for biosensing applications, Plasmonics 6 (2011) 491–506.
[23] R. Shukla, V. Bansal, M. Chaudhary, A. Basu, R.R. Bhonde, M. Sastry, Biocompatibility of gold nanoparticles and their endocytotic fate inside the cellular compartment: a microscopic overview, Langmuir 21 (2005) 10644–10654.
[24] C. Clavero, Plasmon-induced hot-electron generation at nanoparticle/metal-oxide interfaces for photovoltaic and photocatalytic devices, Nat. Photonics 8 (2014) 95–103.
[25] J. Zhang, P. Wang, J. Sun, Y. Jin, High-efficiency plasmon-enhanced and graphene-supported semiconductor/metal core–satellite hetero-nanocrystal photocatalysts for visible-light dye photodegradation and H2 production from water, ACS Appl. Mater. Interfaces 6 (2014) 19905–19913.
[26] J. Lu, J.H. Lu, H. Liu, B. Liu, L. Gong, E.S. Tok, K.P. Loh, C.H. Sow, Microlandscaping of Au nanoparticles on few-layer MoS2 films for chemical sensing, Small 11 (2015) 1792–1800.
[27] S. Su, C. Zhang, L. Yuwen, X. Liu, L. Wang, C. Fan, L. Wang, Uniform Au@ Pt core–shell nanodendrites supported on molybdenum disulfide nanosheets for the methanol oxidation reaction, Nanoscale 8 (2016) 602–608.
[28] W. Liu, B. Lee, C.H. Naylor, H.-S. Ee, J. Park, A.C. Johnson, R. Agarwal, Strong exciton–plasmon coupling in MoS2 coupled with plasmonic lattice, Nano Lett. 16 (2016) 1262–1269.
[29] X. Huang, Z. Zeng, S. Bao, M. Wang, X. Qi, Z. Fan, H. Zhang, Solution-phase epitaxial growth of noble metal nanostructures on dispersible single-layer molybdenum disulfide nanosheets, Nat. Commun. 4 (2013) 1444.
[30] J. Kim, S. Byun, A.J. Smith, J. Yu, J. Huang, Enhanced electrocatalytic properties of transition-metal dichalcogenides sheets by spontaneous gold nanoparticle decoration, J. Phys. Chem. Lett. 4 (2013) 1227–1232.
[31] S.-Y. Cho, H.-J. Koh, H.-W. Yoo, J.-S. Kim, H.-T. Jung, Tunable volatile-organic-compound sensor by using Au nanoparticle incorporation on MoS2, ACS Sensors 2 (2017) 183–189.
[32] P.D. Howes, R. Chandrawati, M.M. Stevens, Colloidal nanoparticles as advanced biological sensors, Science 346 (2014) 1247390.
[33] L. Guo, L. Chen, S. Hong, D.-H. Kim, Single plasmonic nanoparticles for ultrasensitive DNA sensing: from invisible to visible, Biosens. Bioelectron. 79 (2016) 266–272.
[34] P. Anees, S. Sreejith, A. Ajayaghosh, Self-assembled near-infrared dye nanoparticles as a selective protein sensor by activation of a dormant fluorophore, J. Am. Chem. Soc. 136 (2014) 13233–13239.
[35] S. Mariani, S. Scarano, J. Spadavecchia, M. Minunni, A reusable optical biosensor for the ultrasensitive and selective detection of unamplified human genomic DNA with gold nanostars, Biosens. Bioelectron. 74 (2015) 981–988.

[36] L. Yang, H. Mao, Y.A. Wang, Z. Cao, X. Peng, X. Wang, H. Duan, C. Ni, Q. Yuan, G. Adams, Single chain epidermal growth factor receptor antibody conjugated nanoparticles for in vivo tumor targeting and imaging, Small 5 (2009) 235–243.
[37] K.S. Hwang, M.H. Lee, J. Lee, W.-S. Yeo, J.H. Lee, K.-M. Kim, J.Y. Kang, T.S. Kim, Peptide receptor-based selective dinitrotoluene detection using a microcantilever sensor, Biosens. Bioelectron. 30 (2011) 249–254.
[38] Q. Liu, J. Wang, B.J. Boyd, Peptide-based biosensors, Talanta 136 (2015) 114–127.
[39] X. Liu, M. Marrakchi, D. Xu, H. Dong, S. Andreescu, Biosensors based on modularly designed synthetic peptides for recognition, detection and live/dead differentiation of pathogenic bacteria, Biosens. Bioelectron. 80 (2016) 9–16.
[40] J.W. Jaworski, D. Raorane, J.H. Huh, A. Majumdar, S.-W. Lee, Evolutionary screening of biomimetic coatings for selective detection of explosives, Langmuir 24 (2008) 4938–4943.
[41] J.I. Steinfeld, J. Wormhoudt, Explosives detection: a challenge for physical chemistry, Annu. Rev. Phys. Chem. 49 (1998) 203–232.
[42] S. Su, C. Zhang, L. Yuwen, J. Chao, X. Zuo, X. Liu, C. Song, C. Fan, L. Wang, Creating SERS hot spots on MoS2 nanosheets with in situ grown gold nanoparticles, ACS Appl. Mater. Interfaces 6 (2014) 18735–18741.
[43] P.N. Njoki, I.-I.S. Lim, D. Mott, H.-Y. Park, B. Khan, S. Mishra, R. Sujakumar, J. Luo, C.-J. Zhong, Size correlation of optical and spectroscopic properties for gold nanoparticles, J. Phys. Chem. C 111 (2007) 14664–14669.
[44] Y. Cho, B. Cho, Y. Kim, J. Lee, E. Kim, T.T.T. Nguyen, J.H. Lee, S. Yoon, D.-H. Kim, J.h. Choi, Broad-band photocurrent enhancement in MoS2 layers directly grown on light-Trapping Si nanocone arrays, ACS Appl. Mater. Interfaces 9 (2017) 6314–6319.
[45] X. Wang, M. Li, L. Meng, K. Lin, J. Feng, T. Huang, Z. Yang, B. Ren, Probing the location of hot spots by surface-enhanced Raman spectroscopy: toward uniform substrates, ACS Nano 8 (2013) 528–536.
[46] J.-L. Yang, J. Xu, H. Ren, L. Sun, Q.-C. Xu, H. Zhang, J.-F. Li, Z.-Q. Tian, In situ SERS study of surface plasmon resonance enhanced photocatalytic reactions using bifunctional Au@ CdS core–shell nanocomposites, Nanoscale 9 (2017) 6254–6258.
[47] H. Zhang, Y. Ma, Y. Wan, X. Rong, Z. Xie, W. Wang, L. Dai, Measuring the refractive index of highly crystalline monolayer MoS2 with high confidence, Sci. Rep. 5 (2015).
[48] S. Zeng, S. Hu, J. Xia, T. Anderson, X.-Q. Dinh, X.-M. Meng, P. Coquet, K.-T. Yong, Graphene–MoS 2 hybrid nanostructures enhanced surface plasmon resonance biosensors, Sens. Actuators, B 207 (2015) 801–810.
[49] Z. Kuang, S.N. Kim, W.J. Crookes-Goodson, B.L. Farmer, R.R. Naik, Biomimetic chemosensor: designing peptide recognition elements for surface functionalization of carbon nanotube field effect transistors, Acs Nano 4 (2009) 452–458.
[50] I. Popov, G. Seifert, D. Tománek, Designing electrical contacts to MoS 2 monolayers: a computational study, Phys. Rev. Lett. 108 (2012) 156802.
[51] C. Lee, H. Yan, L.E. Brus, T.F. Heinz, J. Hone, S. Ryu, Anomalous lattice vibrations of single-and few-layer MoS2, ACS Nano 4 (2010) 2695–2700.
[52] K.P. Dhakal, D.L. Duong, J. Lee, H. Nam, M. Kim, M. Kan, Y.H. Lee, J. Kim, Confocal absorption spectral imaging of MoS 2: optical transitions depending on the atomic thickness of intrinsic and chemically doped MoS 2, Nanoscale 6 (2014) 13028–13035.
[53] T. Sreeprasad, P. Nguyen, N. Kim, V. Berry, Controlled, defect-guided, metal-nanoparticle incorporation onto MoS2 via chemical and microwave routes: electrical, thermal, and structural properties, Nano Lett. 13 (2013) 4434–4441.
[54] J. Peet, J.Y. Kim, N.E. Coates, W.L. Ma, D. Moses, A.J. Heeger, G.C. Bazan, Efficiency enhancement in low-bandgap polymer solar cells by processing with alkane dithiols, Nat. Mater. 6 (2007) 497–500.
[55] M.E. Stewart, C.R. Anderton, L.B. Thompson, J. Maria, S.K. Gray, J.A. Rogers, R.G. Nuzzo, Nanostructured plasmonic sensors, Chem. Rev. 108 (2008) 494–521.
[56] M.R. Gartia, A. Hsiao, A. Pokhriyal, S. Seo, G. Kulsharova, B.T. Cunningham, T.C. Bond, G.L. Liu, Colorimetric plasmon resonance imaging using nano lycurgus cup arrays, Adv. Opt. Mater. 1 (2013) 68–76.
[57] Y. Li, J.D. Cain, E.D. Hanson, A.A. Murthy, S. Hao, F. Shi, Q. Li, C. Wolverton, X. Chen, V.P. Dravid, Au@ MoS2 core–shell heterostructures with strong light–matter interactions, Nano Lett. 16 (2016) 7696–7702.
[58] L. Yuwen, F. Xu, B. Xue, Z. Luo, Q. Zhang, B. Bao, S. Su, L. Weng, W. Huang, L. Wang, General synthesis of noble metal (Au, Ag, Pd, Pt) nanocrystal modified MoS 2 nanosheets and the enhanced catalytic activity of Pd–MoS 2 for methanol oxidation, Nanoscale 6 (2014) 5762–5769.
[59] S.S. Chou, M. De, J. Kim, S. Byun, C. Dykstra, J. Yu, J. Huang, V.P. Dravid, Ligand conjugation of chemically exfoliated MoS2, J. Am. Chem. Soc. 135 (2013) 4584–4587.
[60] P. Raybaud, J. Hafner, G. Kresse, H. Toulhoat, Adsorption of Thiophene on the catalytically active surface of MoS 2: an ab initio local-density-functional study, Phys. Rev. Lett. 80 (1998) 1481.
[61] K.T. Carron, L.G. Hurley, Axial and azimuthal angle determination with surface-enhanced Raman spectroscopy: thiophenol on copper, silver, and gold metal surfaces, J. Phys. Chem. 95 (1991) 9979–9984.
[62] Q. Zhang, D. Zhang, Y. Lu, Y. Yao, S. Li, Q. Liu, Label-free naked-eye colorimetric biosensing platform based on grapheme oxide/Au nanocomposites for immune detection, Nanomed. Nanotechnol. Biol. Med. 12 (2016) 519.
[63] S. Wang, S. Li, T. Chervy, A. Shalabney, S. Azzini, E. Orgiu, J.A. Hutchison, C. Genet, P. Samorì, T.W. Ebbesen, Coherent coupling of WS2 monolayers with metallic photonic nanostructures at room temperature, Nano Lett. 16 (2016) 4368–4374.
[64] P. Li, Z. Wei, T. Wu, Q. Peng, Y. Li, Au- ZnO hybrid nanopyramids and their photocatalytic properties, J. Am. Chem. Soc. 133 (2011) 5660–5663.
[65] U.O.S. Seker, V.K. Sharma, S. Akhavan, H.V. Demir, Engineered peptides for nanohybrid assemblies, Langmuir 30 (2014) 2137–2143.
[66] Q. Zhang, D. Zhang, Y. Lu, Y. Yao, S. Li, Q. Liu, Graphene oxide-based optical biosensor functionalized with peptides for explosive detection, Biosens. Bioelectron. 68 (2015) 494–499.
[67] H. Khan, T. Barna, R.J. Harris, N.C. Bruce, I. Barsukov, A.W. Munro, P.C. Moody, N.S. Scrutton, Atomic resolution structures and solution behavior of enzyme-substrate complexes of enterobacter cloacae pb2 pentaerythritol tetranitrate reductase multiple conformational states and implications for the mechanism of nitroaromatic explosive degradation, J. Biol. Chem. 279 (2004) 30563–30572.
[68] R. Sodkhomkhum, M. Masik, S. Watchasit, C. Suksai, J. Boonmak, S. Youngme, N. Wanichacheva, V. Ervithayasuporn, Imidazolylmethylpyrene sensor for dual optical detection of explosive chemical: 2, 4, 6-Trinitrophenol, Sens. Actuators, B 245 (2017) 665–673.
[69] D. Zhang, Q. Zhang, Y. Lu, Y. Yao, S. Li, J. Jiang, G.L. Liu, Q. Liu, Peptide functionalized nanoplasmonic sensor for explosive detection, Nano-Micro Lett. 8 (2016) 36–43.
[70] C. Cheng, H.-Y. Chen, C.-S. Wu, J.S. Meena, T. Simon, F.-H. Ko, A highly sensitive and selective cyanide detection using a gold nanoparticle-based dual fluorescence–colorimetric sensor with a wide concentration range, Sens. Actuators, B 227 (2016) 283–290.

Biographies

Jiajia Wu received her bachelor degree at Zhejiang University in 2016. Now she is a Ph.D. student of biomedical engineering of Zhejiang University. Her work includes biosensors and electronic measurements.

Yanli Lu received her Ph.D. degree in biomedical engineering from Zhejiang University in 2017. Now she is a post doctorate in Zhejiang University. Her work includes biosensors and electronic measurements.

Zhiqian Wu received his bachelor degree in Zhejiang University in 2014. Now he is a Ph. D. student of information science and electronic engineering in Zhejiang University. His research area is graphene-like 2D material heterojunction and its optoelectronic device applications.

Shuang Li received her bachelor degree in Hunan normal University in 2014. Now she is a Ph.D. student of biomedical engineering of Zhejiang University. Her work includes biosensors and electronic measurements.

Qian Zhang received her bachelor degree in Zhejiang University in 2012. Now she is a Ph.D. student of biomedical engineering of Zhejiang University. Her work includes biosensors and electronic measurements.

Zetao Chen received his master degree in Yanshan University in 2015. Now he is a Ph.D. student of biomedical engineering of Zhejiang University. His work includes biosensors and electronic measurements.

Jing Jiang received his Ph.D. degree in biomedical engineering from University of Illinois at Urbana-Champaign in 2016. His work includes biosensors and electronic measurements.

Shisheng Lin received his Ph. D. degree in Materials Physics & Chemistry under the joint education of Zhejiang University and Georgia Institute of Technology in 2010. He is currently an Associate Professor in Zhejiang University. Prof. Lin focused on graphene based optoelectronic devices and 2D materials based metamaterials.

Long Zhu received his master degree in Fujian University of Traditional Chinese Medicine. He is currently a Ph.D. student in Fujian University of Traditional Chinese Medicine. His work includes health management and health care administration.

Candong Li received his Ph.D. degree in diagnostics of traditional Chinese medicine from Hunan University of Chinese Medicine, PR China in 2002. He is currently a professor in Fujian University of Traditional Chinese Medicine. He is also the president of Fujian University of Traditional Chinese Medicine, and the chairman of the Health Management Center.

Qingjun Liu received his Ph.D. degree in biomedical engineering from Zhejiang University, PR China in 2006. He is currently a professor in Biosensor National Special Laboratory, Zhejiang University. He is also a visiting scholar in the Micro and Nanotechnology Laboratory (MNTL) at the University of Illinois at Urbana-Champaign (UIUC). He published the book of Cell-Based Biosensors: Principles and Applications, by Artech House Publishers USA in October 2009. His research interests concentrate on the biosensors (e.g. living cell sensor, DNA sensor and protein sensor) and BioMEMS system.